Published by
NIGERIAN SOCIETY OF PHYSICAL SCIENCES
Available online @ https://journal.nsps.org.ng/index.php/jnsps

J. Nig. Soc. Phys. Sci. 7 (2025) 2259

Journal of the Nigerian Society of Physical Sciences

Investigation of the behaviour of tunable chalcogenide-Bismuth based perovskite $BiTl(S_xSe_{1-x})_3(X = 0, 0.33, 0.67, 1)$: first principles calculations

Muteeu A. Olopade[a,*], Anthony B. Adegboyega[a], Kayode I. Ogungbemi[a], Adeyinka D. Adewoyin[b]

[a]*Department of Physics, University of Lagos, Nigeria*
[b]*Physics Unit, Distance Learning Institute, University of Lagos, Nigeria*

Abstract

Density functional theory (DFT) driven by the quantum ESPRESSO code was used in this study to investigate the structural, opto-electronic, and thermoelectric properties of ternary perovskite chalcogenide compound. This is to examine their possible use in optoelectronics and reducing the dependency on silicon and fossil fuel. The Perovskite compounds crystalize in the cubic phase with a space group Pm-3m. The volume versus energy is fitted by the Birch-Murnaghan equation of state which yielded the equilibrium lattice constant of 8.353, 8.488, 8.629 and 8.806, bulk modulus of 255.8, 242.7, 233.5 and 222.4, for $BiTlS_3$, $BiTlS_2Se_1$, $BiTlS_1Se_2$ and $BiTlSe_3$. Indirect band gaps of 2.6 eV, 2.7 eV, 2.9 eV, and 3.2 eV were obtained for $BiTlS_3$, $BiTlS_2Se_1$, $BiTlS_1Se_2$ and $BiTlSe_3$ compounds, respectively. Also, increment in the energy from 0 eV to 10 eV resulted in optical properties fluctuation within 0 cm^{-1} to $1.5 \times 10^9 cm^{-1}$ for absorption coefficient in the compounds. However, a variation from 10 eV to 20 eV moved the absorption coefficient to $4.2 \times 10^9 cm^{-1}$ for all the compounds from visible to the UV range. Furthermore, the observed properties show that the value of figure of merit obtained is 0.125 for $BiTlS_3$, 0.100 for $BiTlS_2Se_1$, 0.068 for $BiTlS_1Se_2$ and 0.055 for $BiTlSe_3$ at 300 K. By adjusting the chalcogen ratio, $BiTlX_3$ (X = S, Se) possess the tunable band gap in the whole visible light range, which is of great significance for the development of new-type, high-efficient semiconductor material and optoelectronic devices, while the low thermoelectric values predict the compounds use as sensors. The proposed results may pave the way for further investigations into the use of the perovskite compounds for optoelectronic devices.

DOI:10.46481/jnsps.2025.2259

Keywords: Chalcogenide based perovskite, Electro-optical properties, Optoelectronics, Thermal sensor, Photovoltaic

Article History :
Received: 18 July 2024
Received in revised form: 05 October 2024
Accepted for publication: 09 October 2024
Available online: 30 October 2024

Communicated by: I. B. Okon

1. Introduction

The dependency on silicon for the production of photovoltaic cells, thermoelectric sensors and dosimeters cannot be overemphasised. However, the cumbersome nature of extracting silicon from sand and the large quantity of material usage have been discouraging. Therefore, there is need to develop new compounds (materials) as substitutes to silicon. Chalcogenide perovskite compounds represent a fascinating class of materials with diverse applications spanning from optoelectronics to energy storage are good substitutes. These compounds are characterized by their unique crystal structure, which mim-

*Corresponding author: Tel.: +234-806-131-1867
Email address: molopade@unilag.edu.ng (Muteeu A. Olopade)

ics the perovskite structure but incorporates elements that are chalcogenides such as sulphur (S), selenium (Se), or tellurium (Te). Sequel to their remarkable qualities, perovskite materials have become attractive options for optoelectronic and thermoelectric devices. The broad range of applications of novel scintillators, including high-energy physics, radiography, environmental security, and other sectors, is currently generating great interest in their research [1]. Room temperature optoelectronic and radiation detector (RTSD) semiconductors that are inexpensive, highly sensitive, and chemically durable are therefore in high demand [2, 3]. The extremely symmetric close-packed materials known as perovskites have been the focus of a great deal of study in recent years because of the diversity of their chemical and physical characteristics. Inorganic-organic halide perovskites have received extraordinary interest in the last several years. Any substance whose crystal structure meets the requirements $AA'BB'X_6$, $A_2BB'X_6$ or ABX_3 is referred to as a perovskite, where X represents a halide or an oxide, (A or A′) indicates a cation or an earth metal, (B or B′) indicates an alkaline earth metal.

Researchers have focused a lot of attention on inorganic lead-free halide-based perovskites because they are promising optoelectronic devices especially when the semiconductor has a band gap in the range 1.5 and 3 eV [4, 5]. Perovskites have demonstrated beneficial uses in light-emitting diodes, indoor solar energy systems, detectors for X-rays, and photocatalysis, to mention a few [6–10]. Comparing halide-based perovskites to their oxide-based counterpart, the former exhibits greater stability against moisture and oxygen because of the absence of organic components [11, 12]. The toxicity of Lead (Pb) to the environment and instability have made lead-based perovskites less widely used in recent years, despite the fact that they have many beneficial technical uses [13, 14]. The work of Ju and his colleagues revealed that chalcogenide perovskites $SrSnSe_3$ and $SrSnS_3$ exhibited good optical properties and tunable bandgaps which are characteristics of potential photovoltaic material [15], Meng *et al.* [16] presented mixed perovskite chalcogenides $BaZr_{1-x}Ti_xS_3$ based on theoretical calculations, also, $BaZrS_3$ and $CaZrS_3$ were synthesized by Perera *et al.* [17] both showing optoelectronic properties. Sun and colleagues computed bandgaps for a broad range of transition metal chalcogenides perovskite with the formula ABX_3 (where X = S, Se; B = Ti, Zr, Hf; and A = Ca, Sr, Ba), presuming a given crystal shape. The abundance of these elements suggested the possibility of producing these materials at a reasonable cost [18].

In this work, we will demonstrate the creative potential of lead-free tunable chalcogenide perovskites for possible optoelectronic applications as well as thermal sensor device which is a novel compound. Al-Qaisi *et al.* recently found that certain lead-free double perovskites have optoelectronic and transport properties. [19–21]. Furthermore, studies conducted by Ali and colleagues show that double perovskite is robust for use in thermoelectric and optoelectronic applications [22–24]. Babu *et al.* [25] investigated a single perovskite $CsCaCl_3$ that possessed the characteristics of an effective scintillator that activates itself. The high density and effective atomic number of thorium-based chloro-perovskites, along with their higher ionizing γ and X-ray detection efficiency, make them a viable substitute for scintillators, according to study by Fujimoto *et al.* [26]. An experimental method described by Wang *et al.* yields a possible future scintillation material when Ce ions are added to double perovskite $Cs_2NaTbCl_6$ [27]. In addition, double perovskite $Cs_2AgBiBr_6$ sensitivity is temperature dependent according to the work of Julian *et al.* [28]. In medical imaging, radiation and particle detection, Zaghrane *et al.* [29] suggest that double perovskite Cs_2LiCeX_6 [X = F, Br, I] is a promising candidate.

The optoelectronic characteristics of PTMC (post transition metal chalcogenide) and TMC (transition metal chalcogenide) materials have not been extensively characterized experimentally till lately. Niu *et al.* [30] synthesized and studied two phases of $SrZrS_3$: the "distorted perovskite" β-phase and the "needlelike" α-phase. Large absorption coefficients and stability at high temperatures were noted.

In this research, the optoelectronic and thermoelectric properties of a tunable chalcogenide-bismuth perovskite compound $BiTl(S_xSe_{1-x})_3$ (X = 0, 0.33, 0.67 and 1) are investigated using density functional theory (DFT). Thereafter, possible applications of the compounds as optoelectronic devices, solar cells, light-emitting diodes, photo detection, and thermal sensor devices will be suggested with respect to the obtained properties.

2. Computational methods

In this work, we utilize the plane-wave and self-consistent (PWSCF) technique based on density functional theory (DFT) [31, 50], which is implemented in the Quantum Espresso software package [32]. Using the generalized gradient approximation of Perdew-Burke-Ernzerholf, we first optimized the crystal structure and calculated the electronic band gaps [33]. Cubic structure of $BiTl(S_xSe_{1-x})_3$ is theoretically optimized by total energy minimization. For the plane-wave basis set expansion, a kinetic energy cut-off of 60 Ry was employed, and for the charge density in the convergence test, 240 Ry. The relaxation of the perovskite complex $BiTl(S_xSe_{1-x})_3$yields new values for the atomic locations and cell dimension.

A 4 × 4 × 4 k-point mesh sampling technique of the Monkhorst-pack was utilized to compute the Brillouin Zone integration; a denser k-mesh of 12 × 12 × 12 was employed for density of state, optical, and thermoelectric computations.

To calculate the thermoelectric characteristics, the BoltzTraP code was utilized, which was developed using the Boltzmann Transport equations [34]. Visualization software package Xcrysden and Grace were used to create the graphs.

3. Results and discussion

3.1. Structural properties

The tunable chalcogenide-bismuth perovskite compound $BiTl(S_xSe_{1-x})_3$ crystallizes in cubic structure (space group Pm-3m) using the Xray diffraction when there is only one chalcogen, but the space group changes to P4/mmm when the chalcogen become two with ratio 1:2. The simulated unit cells for the

Table 1: The lattice parameter a_0(a.u), minimum energy $E_{\min}$ (Ry), bulk modulus B(GPa), equilibrium volume at zero pressure $V_0(a.u)^3$ and band gap energy E_g (eV).

Parameter	$BiTlS_3$	$BiTlS_2Se_1$	$BiTlS_1Se_2$	$BiTlSe_3$
lattice constant $a_0(A^\circ)$	8.353	8.488	8.629	8.806
Bulk modulus B (GPa)	255.8	242.7	233.5	222.4
Volume $V_0(a.u)^3$	145.70	152.87	160.63	170.72
$E_{\min}$ (Ry)	-356.9	-361.8	-366.7	-371.6
Band gap E_g (eV)	2.6	2.7	2.9	3.2

compound with the value of X varying ($X = 0, 0.33, 0.67, 1$) are shown in Figure 1(a-d). The atomic positions in the elementary cell are at Bi (0, 0, 0), Tl (0.5, 0.5, 0.5) and S (0, 0.5, 0.5). Figure 1(a-d) show the crystal structure of $BiTl(S_xSe_{1-x})_3$ using the XCrySDen program [35]. Table 1 shows the lattice constant a_0 a.u., values for the compounds. The computation of lattice parameters is exemplified by equation (1), whereby the Birch-Murnaghan equation of state is used to get the pressure derivative B' and bulk modulus B (GPa). Although there is no literature to compare the compounds with but the observed results show good trend with similar perovskite compounds like $CsPbI_2Br$ (6.40655), Pb_2ScSbO_6 (8.1866), $Cs_2LiCeCl_6$ (10.6750) etc. [36–40]. Figures 1(a-d) display the total energy against the relevant lattice constant. The equation of state is used for the fitting of the total energy at different lattice constants.

$$E(V) = E_0 + \frac{B}{B'(B'-1)}\left[V\left(\frac{V_0}{V}\right)^{B'} - V_0\right] + \frac{B}{B'}(V - V_0). \quad (1)$$

3.2. Electronic properties

The energy minimization process result which is used to identify the arrangement of atoms that results in the lowest possible potential energy for the compounds was used to calculate the band structure and electronic density of state in order to gain a deeper comprehension of the physical characteristics of the materials being studied. This offers crucial details regarding the materials' band gap and can be utilized to predict their optoelectronic applications. The compounds' band structures $BiTlS_3$, $BiTlS_2Se_1$, $BiTlS_1Se_2$ and $BiTlSe_3$ are displayed in Figures 2(a-d) along certain high symmetry lines in the Brillouin zone with the estimated band structure of the compounds.

Figures 2(a-d) show that the four compounds have a suitable band gap according to the established band structure, with an indirect gap, with the peak of the valence band at Γ and the lowest point of the conduction band at R.

As the compound is adjusted by substituting Se for S, the figures demonstrate that band gaps increase in the following order: $BiTlS_3 < BiTlS_2Se_1 < BiTlS_1Se_2 < BiTlSe_3$. The conduction bands move away from the direction of the Fermi level E_f=

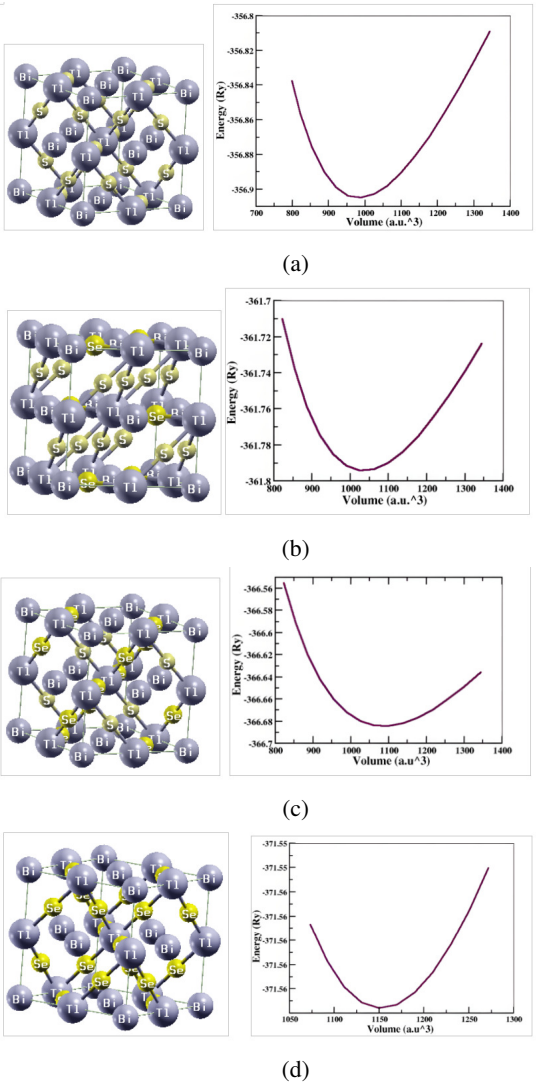

Figure 1: (a) $BiTlS_3$ structure and total energy-lattice parameter. (b) $BiTlS_2Se_1$ structure and total energy-lattice parameter. (c) $BiTlS_1Se_2$ structure and total energy-lattice parameter. (d) $BiTlSe_3$ structure and total energy-lattice parameter.

0) when a chalcogen S is substituted with a chalcogen Se, which explains the rise in the energy gap. The widening of the band gap as a result of tuning the chalcogen make them utilizable in various optoelectronic applications like solar cells, LEDs, Laser Diodes, Photodetectors, Electro-optical modulators etc. for energy is related to the chalcogen size of the molecule since the change affects how the material interact with light which in turn helps predicts its suitability for the listed optoelectronic applications.

For the perovskite compound $BiTl(S_xSe_{1-x})_3$ the band gap for energy are 2.6 eV, 2.7 eV, 2.9 eV, and 3.2 eV, respectively for $BiTlS_3$, $BiTlS_2Se_1$, $BiTlS_1Se_2$ *and* $BiTlSe_3$. The band structure results are supplemented with additional information by the Density of state (DOS) computation. The compound $BiTl(S_xSe_{1-x})_3$has an average bandgap energy of 2.80 eV, which makes it a good fit for possible electro-optical de-

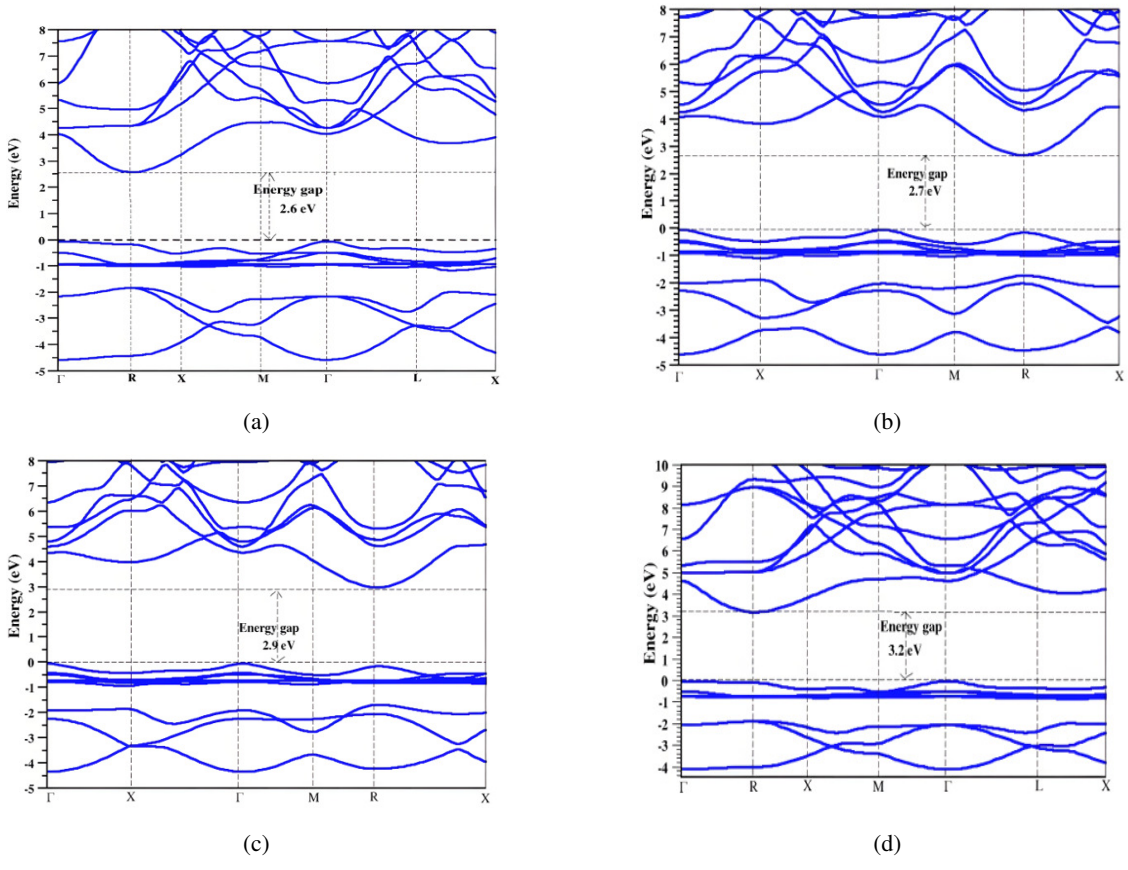

Figure 2: (a) Band structure of $BiTlS_3$. (b) Band structure of $BiTlS_2Se_1$. (c) Band structure of $BiTlS_1Se_2$. (d) Band structure of $BiTlSe_3$.

vice applications. Zero (0) is the value of the fermi energy E_f. The band gap is influenced by both the valence band maximum (VBM) and the conduction band minimum (CBM).

In Figures 3a, 3b, 3c, and 3d, for each of the four compounds, the density of state is displayed. Using DOS calculations, we may determine the separation between energy bands in semiconductors and the overall distribution of states as a function of energy. These energy levels in that order correspond to those in Figures 2a, 2b, 2c, and 2d.

3.3. Optical properties

Predictions of these compounds' optoelectronic applications will be made possible by the examination of their optical characteristics. An electronic material's electron response is described by a complex wave function of dielectric [41], which, in expressed form, is $\varepsilon(\omega) = \varepsilon_1(\omega) + i\varepsilon_2(\omega)$. The component of this equation that is imaginary, $i\varepsilon_2(\omega)$, shows the absorptive activity of the material and is closely linked to its electronic band structure.

The real part of the complex dielectric wave function, $\varepsilon_1(\omega)$, that offers details on the dispersion and polarization of electromagnetic radiations, can be obtained through its imaginary part with the application of the Kramers-Kronig relation. [42, 43]. The reflectivity R (ω), absorption coefficients $\alpha(\omega)$, refractive index $n(\omega)$, optical conductivity $\sigma(\omega)$, energy loss function $L(\omega)$ and extinction coefficient $K(\omega)$ are the remaining optical constants that are computed. The following are the formulas for the given optical parameter:

$$\varepsilon_1(\omega) = 1 + \frac{2}{\pi}\int_0^{\infty} \frac{\omega' \varepsilon_2(\omega)\delta\omega'}{\omega'^2 - \omega^2}, \tag{2}$$

$$\varepsilon_2(\omega) = \frac{-2}{\pi}\int_0^{\infty} \frac{\omega' \varepsilon_2(\omega)\delta\omega'}{\omega'^2 - \omega^2}, \tag{3}$$

$$n(\omega) = \frac{1}{\sqrt{2}}\left(\sqrt{\varepsilon_1^2 + \varepsilon_2^2} + \varepsilon_1\right)^{\frac{1}{2}}, \tag{4}$$

$$k(\omega) = \frac{1}{\sqrt{2}}\left(\sqrt{\varepsilon_1^2(\omega) + \varepsilon_2^2(\omega)} - \varepsilon_1\right)^{\frac{1}{2}}, \tag{5}$$

$$\alpha(\omega) = \sqrt{2}\omega\left(\sqrt{\varepsilon_1^2(\omega) + \varepsilon_2^2(\omega)} - \varepsilon_1(\omega)\right)^{\frac{1}{2}}, \tag{6}$$

$$R(\omega) = \left|\frac{\sqrt{\varepsilon(\omega)} - 1}{\sqrt{\varepsilon(\omega)} + 1}\right|^2, \tag{7}$$

$$\sigma(\omega) = \sqrt{\frac{n^2}{n^2 - 1}}, \tag{8}$$

$$L(\omega) = \frac{\varepsilon_2(\omega)}{\varepsilon_1^2(\omega) + \varepsilon_2^2(\omega)}. \tag{9}$$

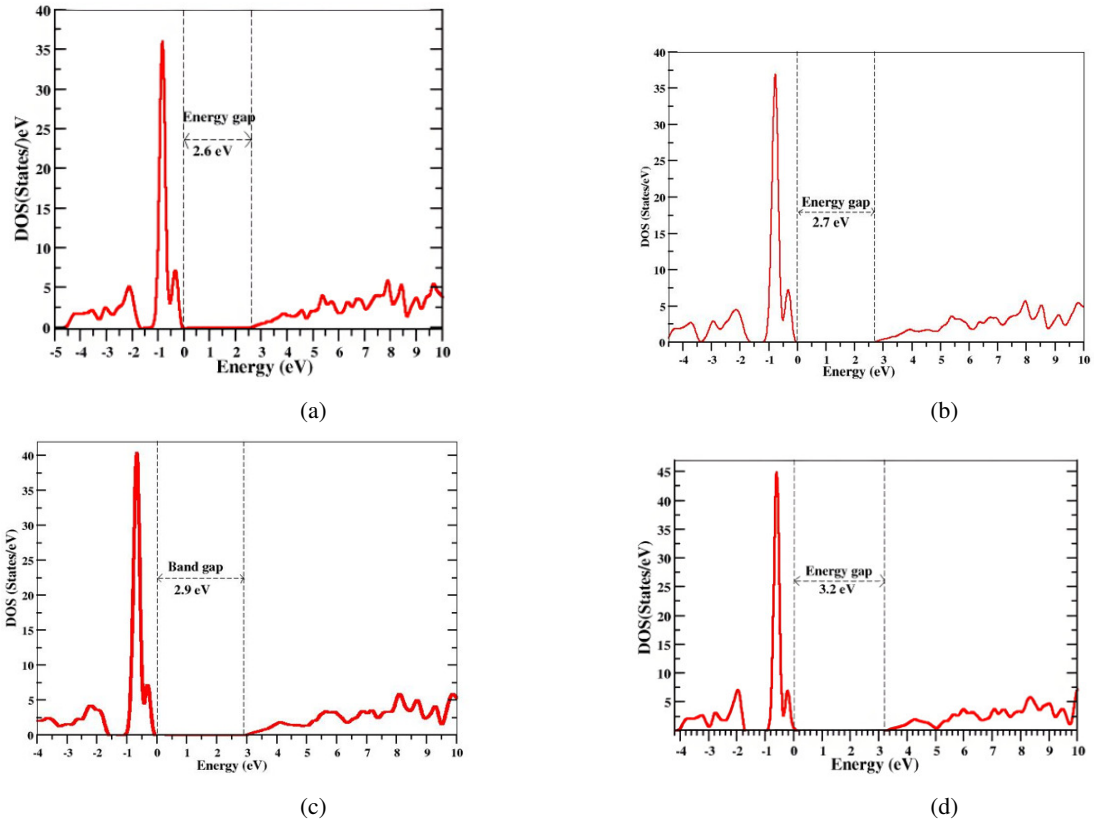

Figure 3: (a) Density of state of $BiTlS_3$. (b) Density of state of $BiTlS_1Se_2$. (c) Density of state of $BiTlS_2Se_1$. Density of state of $BiTlS_1Se_2$. (d) Density of state of $BiTlSe_3$.

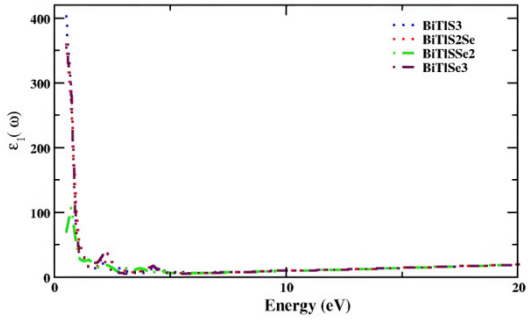

Figure 4: Real dielectric function of $BiTl(S_xSe_{1-x})_3$.

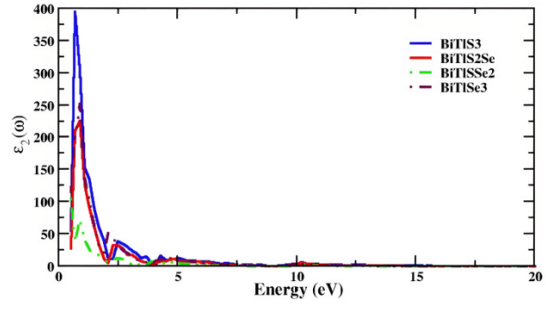

Figure 5: Imaginary dielectric function of $BiTl(S_xSe_{1-x})_3$.

Figures 4-11 display the values computed for the different optical parameters described in the preceding equations with photon energy range of 0–20 eV. $BiTl(S_xSe_{1-x})_3$ compounds' static values for the dielectric constant's real component $\varepsilon_1(\omega)$ are of 410, 365, 75 and 52 at zero frequency for $BiTlS_3$, $BiTlS_2Se_1$, $BiTlS_1Se_2$ and $BiTlSe_3$, respectively. The values decrease fast in the lower energy range to 8.30 (0.92eV), 7.65 (1.1eV), 2.51 (2.86eV), and 1.92 (2.93eV) in respective order as mentioned earlier, all the compounds increased at a very low rate from 1.51 (5.00eV) to 18.21 (20.00eV). The slow rise clearly shows how little polarization and dispersion there is in electromagnetic radiation. The investigated compounds obey the Penn's model. [44]. At zero frequency, the dielectric constant's static values for its imaginary component $\varepsilon_2(\omega)$ for $BiTlS_3$, $BiTlS_2Se_1$, $BiTlS_1Se_2$ and $BiTlSe_3$ were computed as 130. 37, 126.86, 97.61, and 87.61 respectively. The fluctuations between 2eV and 6eV shows the interaction within the electromagnetic spectrum's ultraviolet section. The value of $\varepsilon_2(\omega)$ decreased gradually from 5eV to 20eV which shows that the compounds only weakly absorb light outside of the UV range.

The refractive index n of a material is a measure of how much light slows down and bends when it enters the medium from vacuum or air. The refractive index $n(0)$ static values determined by taking Figure 6 into account are 15.1, 13.9, 10.7,

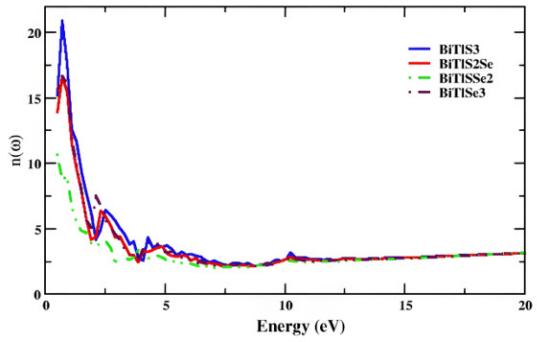

Figure 6: Refractive index $n(\omega)$ of $BiTl(S_xSe_{1-x})_3$.

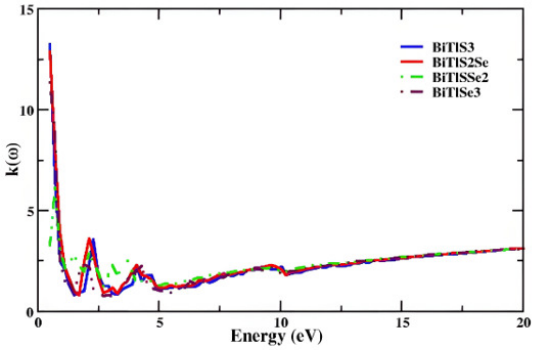

Figure 7: Extinction coefficient of $BiTl(S_xSe_{1-x})_3$.

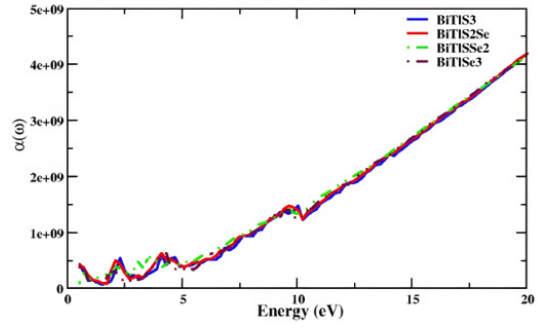

Figure 8: Absorption coefficient of $BiTl(S_xSe_{1-x})_3$.

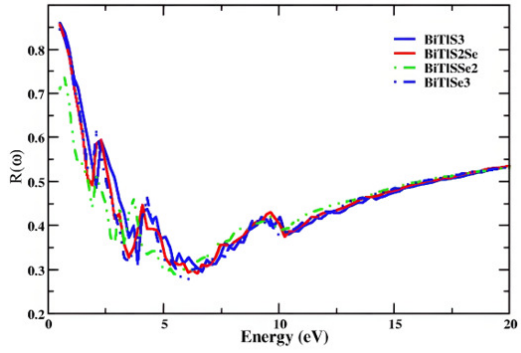

Figure 9: Resistivity of $BiTl(S_xSe_{1-x})_3$.

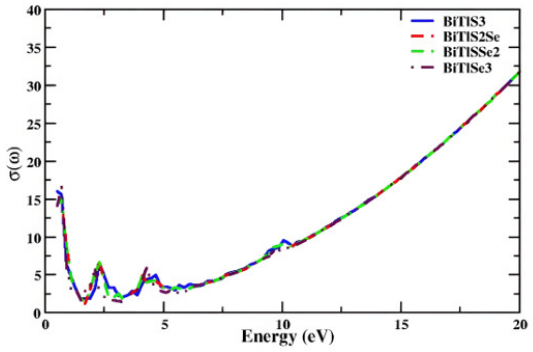

Figure 10: Optical conductivity of $BiTl(S_xSe_{1-x})_3$.

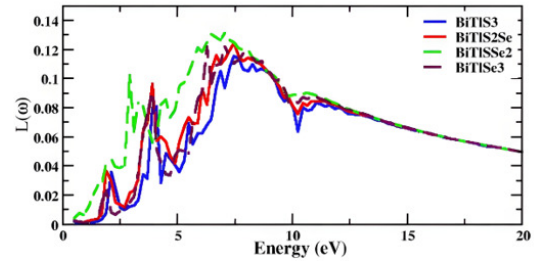

Figure 11: Energy loss of $BiTl(S_xSe_{1-x})_3$.

and 8.4 for $BiTlS_3$, $BiTlS_2Se_1$, $BiTlS_1Se_2$ and $BiTlSe_3$, respectively decreasing linearly to about 5 at 2.4eV. The $n(\omega)$ fluctuates from 5 (2.4eV) to 2.6 (4.3eV), the four compounds rise gradually from 2.6 (4.3eV) to a constant value of 3.1 (20eV). This demonstrates how radiation's interaction with valence electrons results in polarization and a slowing down of light. Another reason is; as the electron density increase, also the value of the refractive increases, but the main relation of the refractive index is with the bonding nature of the material. Usually, ionic compounds show the low value of the refractive index than covalently bonded compounds because in covalent bonding more electrons are shared than that of ionic bonding and correspondingly higher numbers of electrons are distributed in covalent compounds structures and hence there are more chances of the interaction of photons with electrons which results in sufficiently slowing down of the photons. A Higher refractive index in semiconductors helps in confining light and ensuring effective optical interaction within the device. These materials are critical for creating efficient light emission and absorption in optoelectronic devices. Because of their superior optical qualities in the ultraviolet spectrum, the compounds under investigation are deemed acceptable for optical applications based on their refractive index. The refractive index is a complex quantity with real and imaginary parts, the real part, known as the refractive index, describing the phase velocity of light in the medium while the imaginary part, known as the extinction coefficient, describing how much the light is absorbed in the medium.

The extinction coefficient K(ω) indicates how much electromagnetic radiation has been attenuated in a substance. The con-

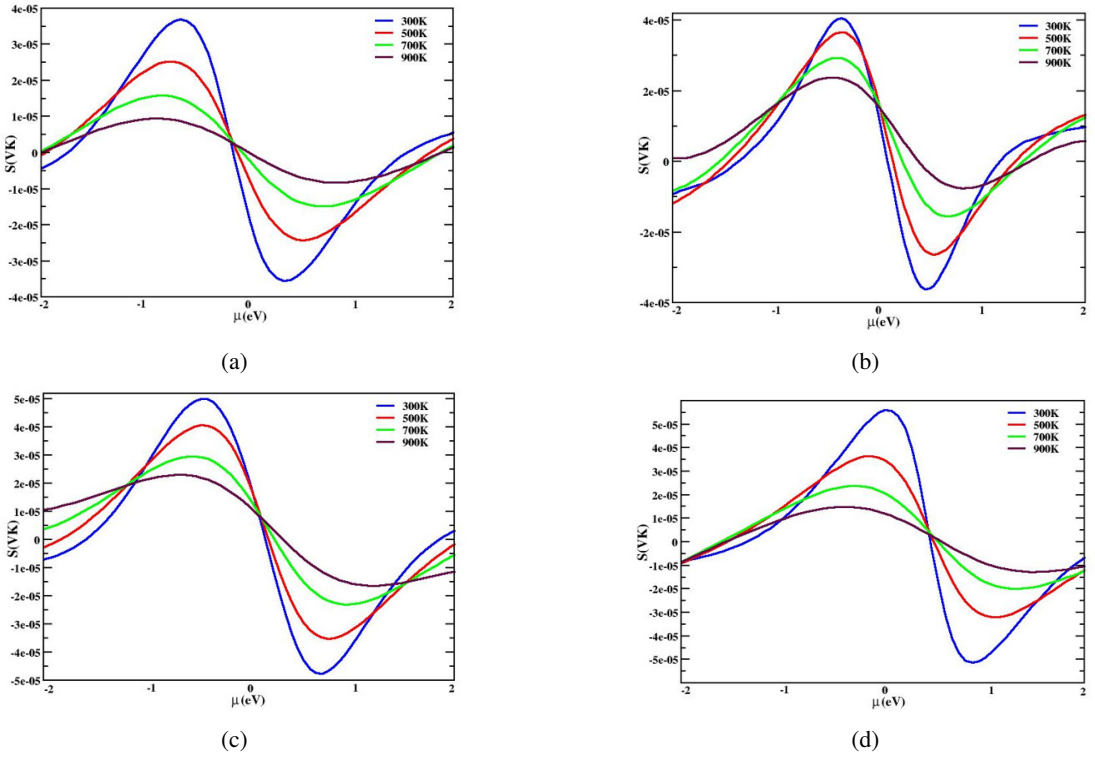

Figure 12: (a) Seebeck coefficient (S) variation for $BiTlS_3$. (b) Seebeck coefficient (S) variation for $BiTlS_2Se_1$. (c) Seebeck coefficient (S) variation for $BiTlS_1Se_2$. (d) Seebeck coefficient (S) variation for $BiTlSe_3$.

stant extinction coefficient values $K(0)$ are 13.2, 12.8, 3.15, and 2.94 for $BiTlS_3$, $BiTlS_2Se_1$, $BiTlS_1Se_2$ and $BiTlSe_3$ respectively, $K(\omega)$ decreased for the four compounds to 1.15 as the energy increased from 0 to 5eV. There is a progressive rise from 1.15 (5eV) to 3.1 (20eV) where $K(\omega)$ reaches the maximum value for the four compounds as depicted in Figure 7. $BiTlS_3$ with a more pronounce value is a better absorber among the compounds. A larger extinction coefficient indicates stronger absorption and, thus, more effective radiation attenuation which is requirement for radiation absorbers and photodetectors.

The quantity of light intensity absorbed in a unit length of a substance is indicated by its absorption coefficient $\alpha(\omega)$. Inner-band transitions are the mechanism by which a photon absorbs when its energy matches the band gap of a compound material. It is directly related to the material's ability to absorb radiation and convert it to other forms of energy (like heat). Significant increase is observed in the UV area and above for all four substances, with a maximum value of $4.2 \times 10^9\ m^{-1}$. Bismuth is primarily responsible for the compounds' strong absorption because of its high absorption coefficient and atomic number which are two essential characteristics for materials to detect radiation [45].

Figure 9 illustrates the reflectance that varies with frequency $R(\omega)$ for different compounds, demonstrating that the formula for calculating the static reflectivity values R(0) is 0.86, 0.85, 0.71, and 0.70 for $BiTlS_3$, $BiTlS_2Se_1$, $BiTlS_1Se_2$ and $BiTlSe_3$, respectively. Regarding each of the four compounds found in the ultraviolet region and beyond, three prominent peaks are distinct with the following values at 2.6 eV, 3.8 eV, and 9.7eV. $R(\omega)$ value increased from 0.38 at 10 eV to 0.54 at 20 eV.

Optical conductivity $\sigma(\omega)$ is a measure of how a material responds to an oscillating electric field (light) at a specific frequency ω. It represents the material's ability to conduct electrical currents in response to the optical field. Like refractive index, optical conductivity can also be a complex quantity, consisting of real and imaginary parts: the real part (representing dissipative effects, like energy loss due to conduction), the imaginary part (representing reactive effects, like energy storage in the medium). Figure 10 displays the material's optical conductivity $\sigma(\omega)$ drops from 17 $\Omega^{-1}cm^{-1}$ at static $\sigma(0)$ to at 1 $\Omega^{-1}cm^{-1}$ at 2.1 eV, a few reactions were noted by the four compounds with $BiTlS_3$ being dominant. at 2.4 eV, 4.3 eV and 10.1 eV which shows the ability to conduct in the ultraviolet region. The peak value of $\sigma(\omega)$ is 32 $\Omega^{-1}cm^{-1}$ showing that higher photon energies excite more electrons to conduct, resulting in an increased optical conductivity.

The energy loss $L(\omega)$ defines the energy loss function during the transition of rapidly moving electrons [46]. Energy losses to non-absorptive processes (like scattering, reflection, or inefficient heat dissipation) negatively impact key optical properties, reducing the overall efficiency of a radiation absorber. For high-performance absorbers: materials with low reflectivity, minimal scattering, and high absorption coefficients are crucial for ensuring maximum energy absorption and conversion in applications like photovoltaics, thermal absorbers, and radiation sensors.

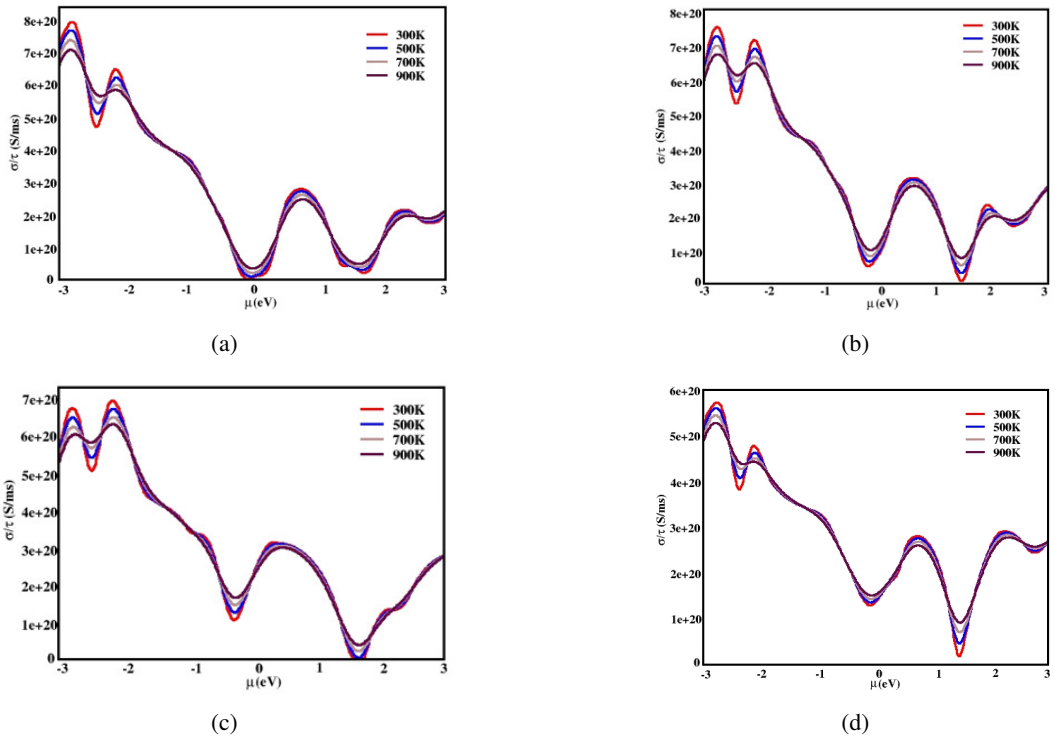

Figure 13: (a) Electrical conductivity σ/τ variation for $BiTlS_3$. (b) Electrical conductivity σ/τ variation for $BiTlS_2Se_1$. (c) Electrical conductivity σ/τ variation for $BiTlS_1Se_2$. (d) Electrical conductivity σ/τ variation for $BiTlSe_3$.

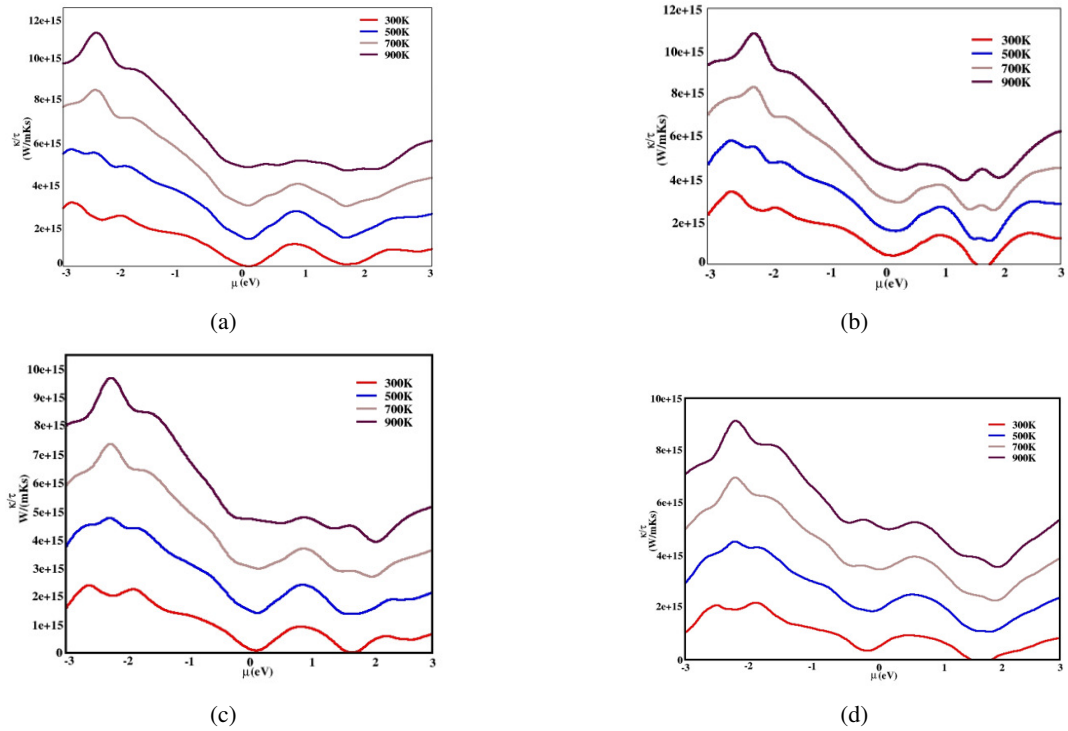

Figure 14: (a) Thermal conductivity κ/τ variation for $BiTlS_3$. (b) Thermal conductivity κ/τ variation for $BiTlS_2Se_1$. (c) Thermal conductivity κ/τ variation for $BiTlS_1Se_2$. (d) Thermal conductivity κ/τ variation for $BiTlSe_3$.

The highest amount of energy lost while interacting with radiation sources is 0.118 at 7 eV for $BiTlS_3$, 0.122 at 7 eV for $BiTlS_2Se_1$, 0.126 at 6.7 eV for $BiTlS_1Se_2$, and 0.130 at 6.8 eV for $BiTlSe_3$ as shown in Figure 11, for all four compounds, the

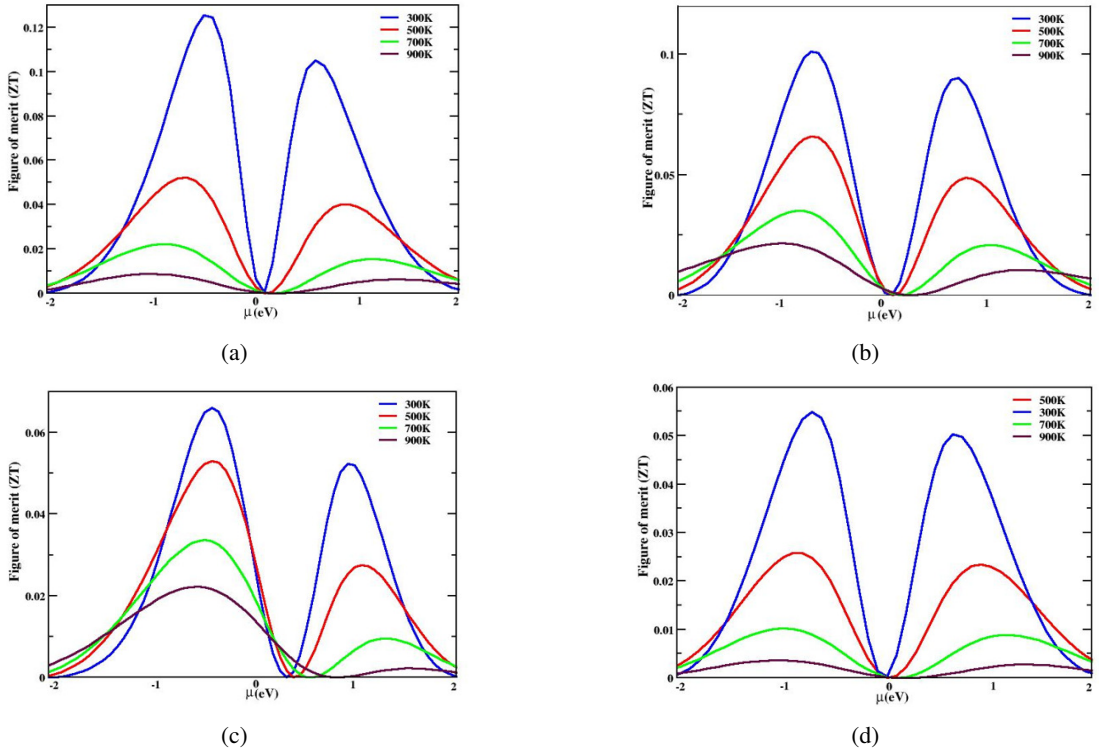

Figure 15: (a) Figure of merit (ZT) variation for $BiTlS_3$. (b) Figure of merit (ZT) variation for $BiTlS_2Se_1$. (c) Figure of merit (ZT) variation for $BiTlS_1Se_2$. (d) Figure of merit (ZT) variation for $BiTlSe_3$.

energy loss is low, suggesting limited scattering.

3.4. Thermoelectric properties

Researchers were motivated to develop novel materials with high conversion ability as indicated by the dimensionless figure of merit (ZT) by this physical occurrence.

Certain transport equations can be directly integrated to get the Seebeck coefficient (S), electrical conductivity σ, and thermal conductivity (κ) [47, 48]. We were intrigued by this information and were inspired to investigate the transport features of the chemical by applying the BoltzTraP algorithm and semi-classical Boltzmann theory. For the temperature value of 300 K, 500 K, 700 K and 900 K the thermoelectric parameters have been computed

$$S_{\alpha\beta}(T,\mu) = \frac{1}{eT\sigma_{\alpha\beta}(T,\mu)} \int \sigma_{\alpha\beta}(\varepsilon)(\varepsilon-\mu)\frac{-\partial f_\mu(T,\varepsilon)}{\partial\varepsilon}d\varepsilon. \tag{10}$$

The potential difference produced in between the extremities of various materials when free electrons move from the upper boundary to the lower boundary temperature is measured by the Seebeck coefficient (S). Figure 12 illustrates how the Seebeck coefficient varies with chemical potential (μ). The Seebeck coefficient falls with increasing temperature, reaching a value of 38 μV/K at 300 K, 25 μV/K at 500K, 15 μV/K at 700 K and 8 μV/K at 900 K for $BiTlS_3$. By replacing S with Se in the compound to get $BiTlS_2Se_1$, $BiTlS_1Se_2$ and $BiTlSe_3$ increased the Seebeck coefficient as displayed in Figures 12a-12d. For the fact that positive values are predominance, the Seebeck coefficient indicates that the conduction is of the p-type.

Electrical conductivity (σ/τ) is a measure of how well a material can conduct electrical current. In thermoelectric materials, high electrical conductivity is important for ensuring efficient charge carrier transport, which is essential for generating electrical power from a temperature gradient or achieving cooling effects via the Peltier effect. Our computed results of electrical conductivity versus chemical potential are plotted for the compounds and are displayed in Figures 13 (a-d). Positive value of chemical potential indicates a n-type doping while negative value of the chemical potential indicates a p-type doping. At room temperature, the values of σ/τ for $BiTlS_3$ is low in the positive region of μ while the value increased to a maximum value of 7.9×10^{20} S/ms in the negative region of μ , corresponding to a p-type doping while a peak intensity 2.5×10^{20} S/ms in observed in the n-type region as displayed in Figure 13a. Accordingly, the σ/τ was influenced by transport distribution function but almost unaffected by the temperature change. Similar plots were observed in Figures 13b-13d when Se replaces S in the compound, showing that σ/τ reduces with increased energy gap.

Likewise, thermal conductivity (κ/τ) parameters are calculated for the compounds and shown in Figures 14 (a-d), it can be seen that κ/τ shows a similar response as σ/τ meaning that maximum and minimum values of electronic thermal conductivity are found in the p-type region and n-type region respectively for the title perovskites due to the direct relationship be-

tween κ/τ and σ/τ according to Wiedemann–Franz law, that is, $\kappa_e = L\sigma T$, where L represents Lorentz number which has a value of $(2.44 \times 10^{-8} J^2 K^{-2} C^{-2})$ as reported in the literature for free electrons [49].

Figure of merit (ZT) is a measure of an ideal or perfect thermoelectric material. Temperature, thermal conductivity, electrical conductivity, and Seebeck coefficient all have role to play in the overall value of the (ZT). The Figure of merit which is directly related to the electrical conductivity also reduces with increasing band gap, since narrow band gap allows electron movement from the valence to the conduction band easier than a wide band gap. Figure 15(a–d) illustrates how the figure of merit sharply drops as temperature rises. With a peak value of 0.125 at 300K, 0.05 at 500K, 0.02 at 700K and 0.008 at 900K for $BiTlS_3$ as shown in Figure 15(a). By replacing S with Se in the compound to get $BiTlS_2Se_1$, $BiTlS_1Se_2$ and $BiTlSe_3$ decreased the figure of merit. The low Figure of merit (ZT) for the compound is due to high thermal conductivity and low Seebeck coefficient.

4. Conclusion

This work has demonstrated that using the first-principles computational technique, a tunable ternary perovskite $BiTl(S_xSe_{1-x})_3$ is attainable. As Se replaces S as the chalcogen, the ground state energy and lattice constant increase considerably. The Investigated materials show semiconducting properties with indirect band gaps of 2.6 eV, 2.7 eV, 2.9 eV and 3.2 eV for $BiTlS_3$, $BiTlS_2Se_1$, $BiTlS_1Se_2$ and $BiTlSe_3$, respectively. The optical characteristics were measured within 0 eV to 20 eV of energy and the compounds possess properties suitable as radiation detectors because of their outstanding absorption coefficient and optical conductivity in the ultraviolet and beyond. Compounds of $BiTl(S_xSe_{1-x})_3$ show great potential for optoelectronic application with respect to the obtained electronic and optical data. The compounds' low Seebeck values make them unsuitable for thermoelectric applications, which produced low figure of merit values of 0.125 for $BiTlS_3$ at 300K, 0.05 at 500 K, 0.02 at 700 K and 0.008 at 900 K. In addition, at room temperature, the figure of merit for the compounds are 0.100 for $BiTlS_2Se_1$, 0.068 for $BiTlS_1Se_2$ and 0.055 for $BiTlSe_3$. Due to low figure of merit, the compounds are suitable as temperature sensors for waste heat recovery in low-power and cooling applications. The newly tunable ternary perovskite explored in this research has promising properties when compared with existing compounds.

References

[1] A. B. Adegboyega, M. A. Olopade, K. I. Ogungbemi & R. O. Balogun, "Electro-optical and thermoelectric properties of perovskite $CsKAgBiX_6$(X = Cl,Br,I): A DFT study", Computational Condensed Matter **38** (2024) e00878. https://doi.org/10.1016/j.cocom.2023.e00878.

[2] X. Li, D. Bi, C. Yi, J. D. Decoppet, J. Luo, S. M. Zakeeruddin, A. Hagfeldt & M. Gratzel, "A vacuum flash–assisted solution process for high-efficiency large-area perovskite solar cells", Science **353** (2016) 58. https://doi.org/10.1126/science.aaf8060.

[3] L. Ma, J. Dai & X. C. Zeng, "Two-Dimensional Single-Layer Organic-Inorganic Hybrid Perovskite Semiconductors", Advanced Energy Materials **7** (2017) 1601731. https://doi.org/10.1002/aenm.201601731.

[4] D. Nason & L. Keller, "The growth and crystallography of bismuth triiodide crystals grown by vapor transport", J. Cryst. Growth **156** (1995) 221. https://doi.org/10.1016/0022-0248(95)00291-X.

[5] P. Ranjan, P. Kumar, T. Chakraborty, M. Sharma & S. Sharma, "A study of structure and electronic properties of chalcopyrites semiconductor invoking Density Functional theory", Mater. Chem. Phys. **241** (2020) 122346. https://doi.org/10.1016/j.matchemphys.2019.122346.

[6] G. Murtaza, I. Ahmad, B. Amin, A. Afaq, M. Maqbool, J. Maqsood, I. Khan & M. Zahid, "Investigation of structural and optoelectronic properties of BaThO3", Optical Materials **33** (2011) 553. https://doi.org/10.1016/j.optmat.2010.10.052.

[7] S. Moskvin, A. A. Makhnev, L. V. Nomerovannaya, N. N. Loshkareva & A. M. Balbashov, "Interplay of p-d and d-d charge transfer transitions in rare-earth perovskite manganites", Physical Review B-Condensed Matter and Materials Physics **82** (2010) 035106. https://doi.org/10.1103/PhysRevB.82.035106.

[8] C. Weeks & M. Franz, "Topological insulators on the Lieb and perovskite lattices", Physical Review B—Condensed Matter and Materials Physics **82** (2010). 085310. https://doi.org/10.1103/PhysRevB.82.085310.

[9] A. Voloshynovskii, P. Savchyn, I. Karbovnyk, S. Myagkota, M. C. Guidi, M. Piccinini & A. I. Popov, "CsPbCl3 nanocrystals dispersed in the Rb0, 8Cs0, 2Cl matrix studied by far-infrared spectroscopy", Solid State Communications **149** (2009) 593. https://doi.org/10.1016/j.ssc.2009.01.032.

[10] Y. Zhou, J. Chen, O. M. Bakr & O. F. Mohammed, "Metal halide perovskites for X-ray imaging scintillators and detectors", ACS energy letters **6** (2021) 739. https://doi.org/10.1021/acsenergylett.0c02430.

[11] J. Liang, C. Wang, Y. Wang, Z. Xu, Z. Lu, Y. Ma, H. Zhu, Y. Hu, C. Xiao & X. Yi, "All-inorganic perovskite solar cells", J. Am. Chem. Soc. **138** (2016) 15829. https://doi.org/10.1021/jacs.6b10227.

[12] Q. Tai, K. C. Tang & F. Yan, "Recent progress of inorganic perovskite solar cells", Energy Environ. Sci. **12** (2019) 2375. https://doi.org/10.1039/C9EE01479A.

[13] J. Yang, C. Bao, W. Ning, B. Wu, F. Ji, Z. Yan, Y. Tao, J. M. Liu, T. C. Sum & S. Bai, "Stable, high-sensitivity and fast-response photodetectors based on lead-free $Cs_2AgBiBr_6$ double perovskite films", Adv. Opt. Mater. **7** (2019) 1801732. https://doi.org/10.1002/adom.201801732.

[14] A. H. Slavney, T. Hu, A. M. Lindenberg & H. I. Karunadasa, "A bismuth-halide double perovskite with long carrier recombination lifetime for photovoltaic applications", J. Am. Chem. Soc. **138** (2016) 2138. https://doi.org/10.1021/jacs.5b13294.

[15] M. Ju, J. Dai, L. Ma & X. C. Zeng, "Perovskite chalcogenides with optimal bandgap and desired optical absorption for photovoltaic devices", Adv. Energy Mater. **7** (2017) 1700216. https://doi.org/10.1002/aenm.201700216.

[16] W. Meng, B. Saparov, F. Hong, J. Wang, D. B. Mitzi, Y. Yan, W. Meng, B. Saparov, F. Hong, J. Wang, D. B. Mitzi & Y. Yan, "Alloying and defect control within chalcogenide perovskites for optimized photovoltaic application", Chemistry of Materials **28** (2016) 821. https://doi.org/10.1021/acs.chemmater.5b04213.

[17] S. Perera, H. Hui, C. Zhao, H. Xue, F. Sun, C. Deng, N. Gross, C. Milleville, X. Xu, D. F. Watson, B. Weinstein, Y. Y. Sun, S. Zhang & H. Zeng, "Chalcogenide perovskites–an emerging class of ionic semiconductors", Nano Energy **22** (2016) 129. https://doi.org/10.1016/j.nanoen.2016.02.020.

[18] Y. Y. Sun, M. L. Agiorgousis, P. Zhang & S. Zhang, "Chalcogenide perovskites for photovoltaics", Nano Lett. **15** (2015) 581. https://doi.org/10.1021/nl504046x.

[19] S. Al-Qaisi, A.M. Mebed, M. Mushtaq, D. P. Rai, T. A. Alrebdi, R. A. Sheikh, H. Rached, R. Ahmed, M. Faizan, S. Bouzgarrou & M. A. Javed, "A theoretical investigation of the lead-free double perovskites halides Rb_2XCl_6 (X = Se, Ti) for optoelectronic and thermoelectric applications", J. Comput. Chem. **44** (2023) 1690. https://doi.org/10.1002/jcc.27119.

[20] S. Al-Qaisi, Q. Mahmood, N. A. Kattan, S. Alhassan, T. Alshahrani, N. Sfina, S. Brini, A. Hakamy, A. Mera & M. A. Amin, "Tuning of band gap by variation of halide ions in K_2CuSbX_6 (X = Cl, Br, I) for solar cells and thermoelectric applications", J. Phys. Chem. Solid **174** (2023) 111184. https://doi.org/10.1016/j.jpcs.2022.111184.

[21] S. Al-Qaisi, H. Rached, T. A. Alrebdi, S. Bouzgarrou, D. Behera, S.K. Mukherjee, M. Khuili, M. Adam, A. S. Verma & M. Ezzeldien, "Study of mechanical, optical, and thermoelectric characteristics of Ba_2XMoO_6 (X = Zn, Cd) double perovskite for energy harvesting, J. Comput. Chem. **44** (2023) 2442. https://doi.org/10.1002/jcc.27209.

[22] M. A. Ali, M. Musa Saad H. E., A. M. Tighezza, S. Khattak, S. Al-Qaisi & M. Faizan, "First-principles calculations of novel lead-free X_2GeSnI_6 (X=Rb, Cs) double perovskite compounds for optoelectronic and energy exploitations", Journal of Inorganic and Organometallic Polymers and Materials **34** (2024) 1. http://dx.doi.org/10.1007/s10904-023-02901-8.

[23] A. M. Mebed, M. Mushtaq, I. Muhammad, I. N. Lone, S. AL-Qaisi, N. Algethami, E. F. EL-Shamy, A. Laref & N. M. AL-Hosiny, "Structure, half-metallic and magnetic properties of bulk and (001) surface of Rb_2XMoO_6 (X = Cr, Sc) double perovskites: a DFT + U study", Phys. Scripta **98** (2023) 015807. https://doi.org/10.1088/1402-4896/aca56b.

[24] H. Albalawi, S. A. Rouf, T. Zelai, N. A. Kattan, S. Bouzgarrou, Q. Mahmood, S. AlQaisi & E. Yousef, "The study optical, thermoelectric, and thermodynamic properties of double perovskites K_2CuBiX_6 (X = Cl, Br, I) for energy harvesting", Mater. Sci. Eng. B **298** (2023) 116851. https://doi.org/10.1016/j.mseb.2023.116851.

[25] K. Ephraim Babu, N. Murali, K. Vijaya Babu, P. Taddesse Shibeshi & V. Veeraiah, "Structural, elastic, electronic, and optical properties of cubic perovskite $CsCaCl_3$ compound: an ab initio study", Acta Phys. Pol. A **125** (2014) 1179. https://doi.org/10.12693/APhysPolA.125.1179.

[26] Y. Fujimoto, M. Koshimizu, T. Yanagida, G. Okada, K. Saeki & K. Asai, "Thallium magnesium chloride: a high light yield, large effective atomic number, intrinsically activated crystalline scintillator for X-ray and gamma-ray detection", Jpn. J. Appl. Phys. **55** (2016) 090301. https://doi.org/10.7567/JJAP.55.090301.

[27] Z. Wang, X. Xu, S. Wang, Hui Xu, Weiwei Xu, Q. Zeng, G. Deng, Y. Jiang & S. Wu, "Cerium doping double perovskite scintillator for sensitive X-ray detection and imaging", Chem. Eur. J. **27** (2021) 9071. https://doi.org/10.1002/chem.202100449.

[28] J. A. Steele, W. Pan, C. Martin, M. Keshavarz, E. Debroye, H. Yuan, S. Banerjee, E. Fron, D. Jonckheere, C. W. Kim, W. Baekelant, G. Niu, J. Tang, J. Vanacken, M. V. Auweraer, J. Hofkens & M. B. J. Roeffaers, "Photophysical pathways in highly sensitive $Cs_2AgBiBr_6$ double-perovskite single-crystal X-ray detectors", Adv. Mater. **30** (2018) 1804450. https://doi.org/10.1002/adma.201804450.

[29] A. Zaghrane, H. Ouhenou, E. M. Agouri, A. Abbassi, Y. Mekaoui, S. Taj & B. Manaut, "First-principles investigation of structural, electronic, optical, and magnetic properties of a scintillating double perovskite halides (Cs_2LiCeX_6) with (X = F, Br, and I)", Chin. J. Phys **90** (2023) 111. https://doi.org/10.1016/j.cjph.2023.08.001.

[30] Niu, H. Huyan, Y. Liu, M. Yeung, K. Ye, L. Blankemeier, T. Orvis, D. Sarkar, D. J. Singh & R. Kapadia, "Bandgap control via structural and chemical tuning of transition metal perovskite chalcogenides", Adv. Mater. **29** 1604733 (2016). https://doi.org/10.1002/adma.201604733.

[31] L.J. Sham & W. Kohn, "One-particle properties of an inhomogeneous interacting electron gas", Phys. Rev. **145** (1966) 561. https://doi.org/10.1103/PhysRev.145.561.

[32] P. Giannozzi, S. Baroni, N. Bonini, M. Calandra, R. Car, C. Cavazzoni, D. Ceresoli, G. L. Chiarotti, M. Cococcioni & I. Dabo, "Quantum espresso: a modular and open-source software project for quantum simulations of materials", J. Phys. Condens. Matter **21** (2009) 395502. https://iopscience.iop.org/article/10.1088/0953-8984/21/39/395502.

[33] J. P. Perdew, K. Burke & M. Ernzerhof, "Generalized gradient approximation made simple", Phys. Rev. Lett. **77** (1996) 3865. https://doi.org/10.1103/PhysRevLett.77.3865.

[34] G. K. H. Madsen & D. J. Singh, "BoltzTraP. A code for calculating band-structure dependent quantities", Comput. Phys. Commun. **175** (2006) 67. https://doi.org/10.1016/j.cpc.2006.03.007.

[35] K. Anton, "Computer graphics and graphical user interfaces as tools in simulations of matter at the atomic scale", Computational Materials Science **28** (2003) 155. https://doi.org/10.1016/S0927-0256(03)00104-6.

[36] S. Bouhmaidi, A. Azouaoui, N. Benzakour, A. Hourmatallah & L. Setti, "First-principles calculations on structural, electronic, elastic, optical and thermoelectric properties of thallium based chloroperovskites $TlMCl_3$ (M= Zn and Cd)", Computational Condensed Matter **33** (2022) e00756. https://doi.org/10.1016/j.cocom.2022.e00756.

[37] Hnamte, Lalhriatpuia, Himanshu Joshi & R. K. Thapa, "Electronic and optical properties of double Perovskite oxide Pb_2ScSbO_6: a first principles approach", IOSR J. Appl. Phys. **10** (2018) 39. https://doi.org/10.9790/4861-1003023944.

[38] C. Han, M. Li, B. Wang, S. Ming & J. Su, "Structure, electronic and optical properties of $CsPbX_3$ halide perovskite: a first-principles study", Journal of Alloys and Compounds **862** (2021) 158442. https://doi.org/10.1016/j.jallcom.2020.158442.

[39] G. Rooh, H. J. Kim & S. Kim, "Study on crystal growth and scintillation characteristics of $Cs_2LiCeCl_6$, IEEE Trans. Nucl. Sci. **57** (2010) 1255e9. https://doi.org/10.1109/TNS.2009.2037903.2.

[40] P. R. Bennet, K. S. Shah, L. J. Cirignano, M. B. Klugerman, L. P. Moy & M. R. Squillante, "Characterization of polycrystalline TlBr films for radiographic detectors", IEEE Trans. Nucl. Sci. **46** (1999) 266. https://doi.org/10.1109/23.775525.

[41] A. Srivastava, P. Sarkar & S. K. Tripathy, "Structural, electronic and optical properties of $Ag_2MgSn(S/Se)_4$ quaternary chalcogenides as solar cell absorber layer: an Ab-initio study", Solar Energy **209** (2020) 206. https://doi.org/10.1016/j.solener.2020.08.094.

[42] Y. Grabovsky & N. Hovsepyan, "On the feasibility of extrapolation of the complex electromagnetic permittivity function using Kramers--Kronig relations", SIAM Journal on Mathematical Analysis **53** (2021) 6993. https://doi.org/10.1137/20M1369427.

[43] B. Gralak, M. Lequime, M. Zerrad & C. Amra, "Phase retrieval of reflection and transmission coefficients from Kramers–Kronig relations", JOSA A **32** (2015) 456. https://doi.org/10.1364/JOSAA.32.000456.

[44] D. R. Penn, "Wave-number-dependent dielectric function of semiconductors", Phys. Rev. **128** (1962) 2093. https://doi.org/10.1103/PhysRev.128.2093.

[45] P. Sharma & S. C. Katyal, "Determination of optical parameters of a-(As2Se3) 90Ge10 thin film", Journal of Physics D: Applied Physics **40** (2007) 2115. https://doi.org/10.1088/0022-3727/40/7/038.

[46] E. W. Van Stryland & D. R. Williams, *Handbook of optics*, Vol. 2, McGraw-Hill, New York, 1995, pp. 33-66. https://doi.org/10.1036/0071414789.

[47] S. Bouhmaidi, A. Marjaoui, A. Talbi, M. Zanouni, K. Nouneh & L. Setti, "A DFT study of electronic, optical and thermoelectric properties of Ge-halide perovskites $CsGeX_3$ (X=F, Cl and Br)", Computational Condensed Matter **31** (2022) e00663. https://doi.org/10.1016/j.cocom.2022.e00663.

[48] M. Rizwan, H. M. N. Ullah, S. S. Ali, U. Hira, H. Naeem & Z. Usman, "Quantum mechanical investigation of the structural stability, pressure-induced thermoelectric response, electronic and optical behaviour of $SrZrO_3$ under extreme conditions. (2023). [Online]. https://doi.org/10.21203/rs.3.rs-3083894/v1.

[49] Jonson, M. & G. D. Mahan, "Mott's formula for the thermopower and the Wiedemann-Franz law", Physical Review B **21** (1980) 4223. https://doi.org/10.1103/PhysRevB.21.4223.

[50] Babalola, M. I., B. E. Iyorzor & S. O. Ebuwa. "First principles calculation of half metallic proprieties of QCrAs (Q= Hf, Ti and Zr)", Journal of the Nigerian Society of Physical Sciences **5** (2023) 1029. https://doi.org/10.46481/jnsps.2023.1029.